Thesis Title

A subtitle of your thesis

Author name

Thesis submitted for the degree of
Master in Master's Program Name <change at main.tex>
60 credits

Department Name <change at main.tex>
Faculty name <change in duoforside.tex>

UNIVERSITY OF OSLO

Spring 2022

Thesis Title

A subtitle of your thesis

Author name

Thesis Title

http://www.duo.uio.no/

Printed: Reprosentralen, University of Oslo

Abstract

Contents

List of Figures

List of Tables

Preface

Chapter 1

Introduction

some introduction on the importance of discovering new materials and alloying.
Need something on thermoelectricity related to both the band gap and high-entropy alloys.

High-entropy alloys is a novel class of materials based on alloying multiple components, as opposed to the more traditional binary alloys. This results in an unprecedented opportunity for discovery of new materials with a superior degree of tuning for specific properties and applications. Recent research on high-entropy alloys have resulted in materials with exceedingly strong mechanical properties such as strength, corrosion and temperature resistance, etc **find references**. Meanwhile, the functional properties of high-entropy alloys is vastly unexplored. In this study, we attempt to broaden the knowledge of this field, the precise formulation of this thesis would be an exploration on the possibilities of semiconducting high-entropy alloys.

A key motivation of this thesis is the ability to perform such a broad study of complex materials in light of the advances in material informatics and computational methods. In this project, we will employ Ab initio methods backed by density functional theory on top-of the line supercomputers and software. 20 years ago, at the breaking point of these methods, this study would have been significantly narrower and less detailed firstly, but secondly would have totaled ... amount of CPU hours to complete (**Calculate this number**). In the addition to the development in computational power, is also the progress of modeling materials, specifically we will apply a method called Special Quasi-random Structures (SQS) to model high-entropy alloys or generally computationally complex structures. Together with the open landscape of high-entropy alloys described above, these factors produce a relevant study in the direction of applying modern computational methods to progress the research of a novel material class and point to promising directions for future research.

In specifics, this thesis revolve around the electrical properties of high-entropy alloys, mainly the band gap as this is the key indicator for a semiconducting material and it's applicability. Semiconductors are the building blocks in many different applications in today's world, ranging

from optical and electrical devices, to renewable energy sources such as solar and thermoelectricity. Given the economic and sustainable factors concerning silicon, in addition to its role in relevant applications such as microelectronics and solar power. Silicon emerges as a natural selection to build our alloys around. Furthermore, the development and research on both high entropy alloys and metal silcides have been heavily centered around 3d transition metals. Keeping in line with the economic and environmental factors, we will continue this direction by focusing on high entropy stabilized sustainable and economic 3d metal silicides **Not happy with this writing**. Throughout the study we will analyze a great number of permutations of 3d silicides, from different initial metal silicides such as $CrSi_2$, $FeSi_2$, $MnSi_{1.75}$, Fe_2Si, each with distinct properties relating to the band gap, crystal structure and metal to silicon ratio. In addition, the permutations include numerous metal distributions and elements within the 3d-group of metals. Examples are Co, Cr, Fe, Mn, and Ni.

Given a background in high-entropy alloys, one could ask if this study is truly sensible. In the later sections we will cover the details of this field, and it quickly become clear that the materials investigated in this study does not fall under the precise definition of high-entropy alloys, nor do we intend to explore the properties and factors relating to high-entropy stabilized alloys such as the configurational entropy, phase stability and finite temperature studies. However this study is motivated from the discovery of these materials and promising properties, and venture into a more hypothetical space of materials, enabled by the computational methods available to study the potential properties of such materials. On the other hand, very recent studies **Mari, and other HEA silicide study** have experimentally synthesized high-entropy disilicides, thus in some way justifying the direction of this project.

We begin this project by reviewing key concepts of solid-state physics for readers lacking a background in materials science, and an introduction to the base 3d silicides of the experimental work. Later follows a theoretic walk-through of the relevant concepts of this thesis, these topics include high-entropy alloys, special quasi-random structures, and density functional theory. Next we shine light on the implementation of DFT in this project, and other computational details required to reproduce the results in this thesis, such as the use of the Vienna Ab Initio Simulation Package (VASP) and implementation of SQS. Finally we present the results of our study, these include the band gap and electronic properties of various structures and the success and challenges of the computational methods applied throughout the study.

Part I

Theory

Part II

Methodology and Implementation

Part III

Results and Discussion

Trenger jeg denne biten? Evt hvor? In this one year long project, we have collected results of a great number of materials with various structures and compositions. The initial experimentation was based on high-entropy silicides of the Fe_2Si unit cell, created from the special quasi-random structure approach as described above. Despite the non-semiconducting character of this compound, we worked under the idea that the extraordinary properties that have been observed in high-entropy alloys through effects such as the cocktail effect, we could discover specific combinations of elements that would yield a semiconductor. In addition, the ratio between silicon atoms to metals allowed us to create nearly eqvimolar high-entropy alloys.

Following this attempt, we transistioned into studying high-entropy silicides based on well known semiconducting 3d silicides such as $\beta-FeSi_2$, $CrSi_2$ and $MnSi_{1.75}$. The main outcome of this project is that for all 4 different starting silicides, we could only produce high-entropy silicides from one unit cell, furthermore in this cell only one specific compositions of elements was semiconducting. This was $Cr_{0.25}Fe_{0\cdot 25}Mn_{0.25}Ni_{0.25})Si_2$, herein CFMN, in the $\beta-$ $FeSi_2$ crystal structure.

This section will be structured in the following manner, firstly we will investigate the CFMN (fesi2) compound and various permutations of the composition. Thereafter we will look at other possible compositions of fesi2 based high-entropy silicides, and lastly test the CFMN composition in other crystal symmetries. In final we will present an overview of the complete study and the various compounds that have been investigated in order to propose promising directions and guideline future research directions in this field. In this way, we aim to understand the uniqe properties of CFMN (fesi2) and why this particular compound is semiconducting compared to the other testes structures in this project. Properties we will cover is the overall stability by total energy and corresponding enthalpy of formation, the magnetic properties and which elements contribute to the magnetism. But in majority, we will look at the band gap and related properties, as this is the main motivation and distinction of the study.

Chapter 8

The good (CFMN fesi2)

Add figure of LDOS around Ef for SQS B to compare with sqs D. Also change the name from local DOS to projected DOS and explain the assumption regarding 3d electrons and why we did not include plots of the local DOS. $\beta - FeSi_2$ in the orthorombic cmce crystal lattice is a well known semiconductor with an experimentally measured band gap of around 0.8 ev **cite**, the nature of the band gap is under debate, all though most ab inito studies point to an indirect gap, experimental work indicate a direct gap. From our own DFT calculations, we find an indirect band gap close to 0.65 eV with PBE. This is in good agreement with other meassurements from ab intitio studies **cite materials projects, other studies.**

The density of states and charge density of bulk $\beta-\mathrm{FeSi_2}$ from PBE calculations can be seen in figure .., .. From the figures we observe a clear band gap and semiconducting character. Moreover, we note from the density of states that the gap is identical in both spin channels, indicating that this material is diamagnetic. We find this to be true from the written magnetization in VASP, this also is in agreement with relevant literature **cite**. **Find reference for stability and** ΔH^0**.** Finally, the enthalpy of formation of this compound is -18.6583 eV.

8.1 CFMN Eqvimolar distribution

8.1.1 Introduction

The CFMN alloys of the fesi2 unit cell alloys can be seen in figure ... The supercells consist of 48 atoms, 16 of which is evenly distributed between Cr, Fe, Mn, and Ni, the remaining 32 sites occupied by silicon atoms. Bellow in table .. we list the total energy per atom (Toten), final magnetic moment per atom (Mag), and the band gap of the five distinct SQSs corresponding to the CFMN (fesi2) compound. In addition we include the mean and standard deviation of the values, plus the enthalpy of formation. For simplicity, we denote the SQSs as A, B, C, D and E.

Structure	Toten (eV)	Mag (?)	Band gap (eV)
A	-6,6080	0.0833	0.0280
B	-6,6138	0.0833	0.0523
C	-6,6063	0.0834	0.0344
D	-6,6155	0.0833	0
E	-6,6089	0.0833	0.0495
Mean	-6.6105	4.0000	0.0328
Std	0.0039	0.0000	0.0210
ΔH^0_{mean}	-11.5000 eV	-	-

Table 8.1: Total energy per atom, final magnetic moment, band gap (GGA) and formation enthalpy of $Cr_4Fe_4Mn_4Ni_4Si_{32}$ SQSs based on $FeSi_2$

Write a section on magnetism in method From a first glance, we observe very similar properties between the SQSs regarding both the total energy and final magnetic moment. Comparing to bulk $FeSi_2$, this compound is both less stable, from the enthalpy of formation, and magnetic. For the magnetic character of the compound, we performed self-consistent total energy calculations with three diffrent magnetic configurations, non-magnetic (ispin=1), colinear magnetism with the initial magnetic moment equal to 1 times the number of ions, and lastly two times N ions. Of the three starting positions, we found the two latter to yield near identical total energies, with the middle seting winning out in some SQSs. The consistent magnetic moment between the 5 supercells is excpected seeing as all 5 structures consist of equivalent elements. The magnetic moment observed is solely attributed from 3d electrons and in particular those of chromium and manganese atoms.

8.1.2 The band gap

The most interesting property of these SQSs is in fact the band gap. We note a mean band gap of about 0.03 eV, much lower than 0.65 eV of bulk $FeSi_2$. But a band gap in this smaller range makes for excellent application in for instance thermoelectrics. The gap is seen in 4 out of 5 SQSs, but surprisingly not in the most stable arrangement (D), the largest gap observed is about 0.05 eV from structure B, which is slighlty bellow D in terms of total energy, but still a way above the mean energy. Similar to the bulk material, also these band gaps are indirect, the transitions are listed bellow in table .. .

Structure	Gap (D/I)	Transition
A	I	(0.500,0.333,0.500) → (0.500,0.000,0.000)
B	I	(0.250,0.000,0.250) → (0.000,0.000,0.000)
C	-	(0.500,0.000,0.500) → (-0.250,0.333,0.500)
D	I	-
E	I	(0.000,0.000,0.000) → (0.250,0.000,0.250)

Table 8.2: Band gap transition of CFMN (fesi2) SQSs with PBE functional

A very useful method to extract information regarding the band gap of a material is to plot and study the band structure, however this is not as insightful when considering large supercells consisting of several elements and a large number of energy bands. The solution to this is normally to do a band unfolding, but given the complex structure and implementation of SQSs in VASP proved difficult. Instead we investigate the band gap from the plotted density of states shwon in figure 8.1. We only include the DOS of this particular super-cell because results of the most stable arrangement is probably the most representative of a potential high-entropy silicide, nevertheless we will consider the remaining SQSs in the following sections as well.

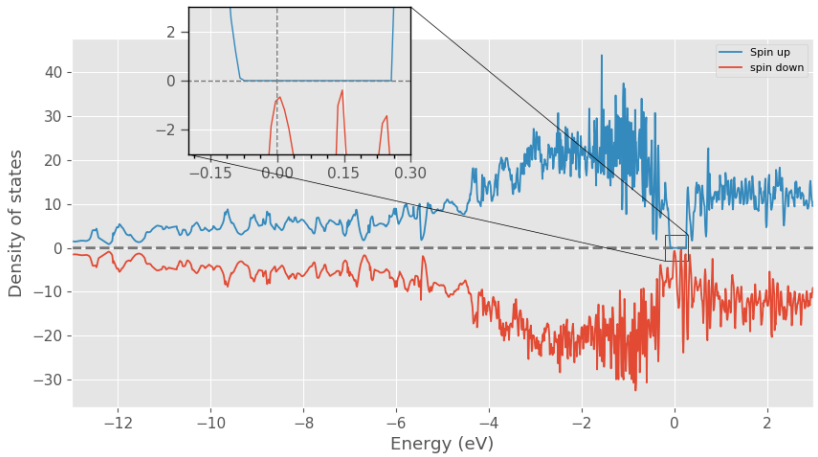

Figure 8.1: Density of states SQS D CFMN (fesi2) from PBE calculation

From the DOS we observe that the band gap in this structure differ between the spin up states and spin down states, following the magnetic property of the material seen in table 8.1. In this particular SQS the spin down channel is completely metallic, and the spin up channel exhibit a relatively large band gap, thus we can classify this SQS as either a half-metal, or possibly a spin-gapless conductor (**Insert references/discuss this**). Furthermore we find that the band gap in all SQSs of this alloy is severely spin-polarized in the spin up direction **Is this okay to say?**. We list the spin-dependent band gaps in table 8.3, and show the relationship in SQS B in figure 8.2 bellow.

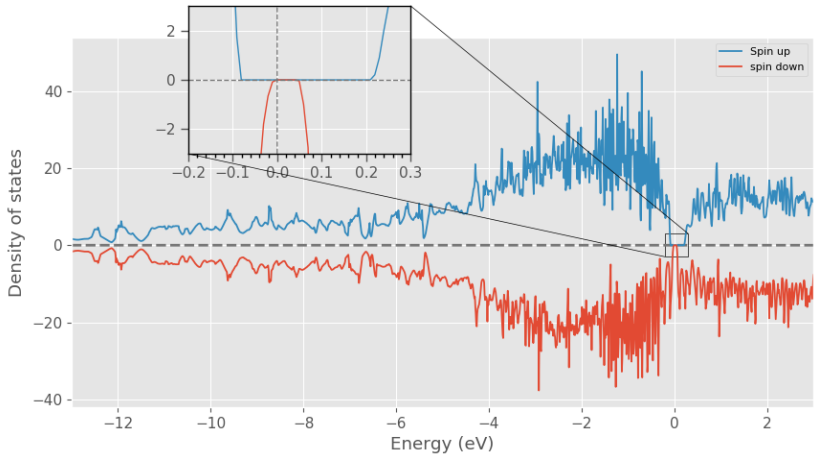

Figure 8.2: Density of states SQS B CFMN (fesi2) from PBE calculation

Structure	Spin-up	Spin-down	Total
A	0.0814	0.0522	0.0281
B	0.2932	0.0523	0.0523
C	0.2355	0.0343	0.0343
D	0.3386	0	0
E	0.3078	0.0495	0.0495

Table 8.3: Band gap (eV) with PBE in spin up and spin down channels of CFMN (fesi2) SQSs

From table 8.3 we find that SQSs B D and E all display band gaps around 0.3 eV in spin up, and small non-zero or zero in the case of SQS D in spin down. To further explore the electronic structure we plot both the projected density of states and local density of states of SQS D. With this information we can study the above case by the contributions of individual elements in the structure. From the local density of states plotted in figures 8.3 and 8.4 we see that the s-electrons in Si occupy states in the lower energy regions and the p electrons at energies closer to the Fermi energy, while both equally occupy states above E_F. In the transition metals we see that 3d electrons dominate across the energy range. Between the different TMs we observe that 3d electrons particularly of manganese and chromium show a strong presence in spin down right above E_F, and just bellow in the spin up direction. Meanwhile iron and nickel lie at lower energies respectively. The relationship and interaction between the different elements can better be seen in the projected density of states in figure 8.5.

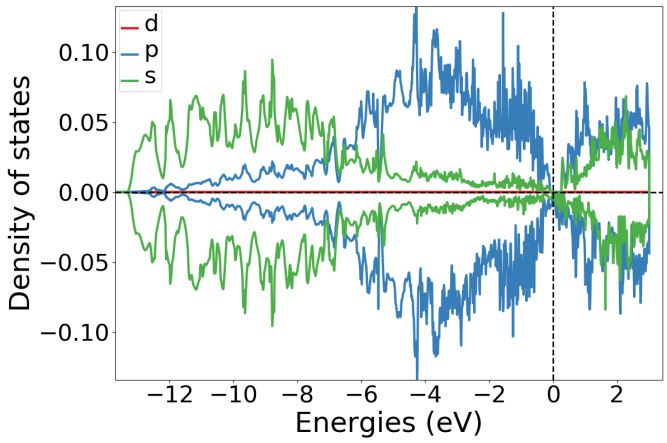

Figure 8.3: Local density of states of Si (SQS D)

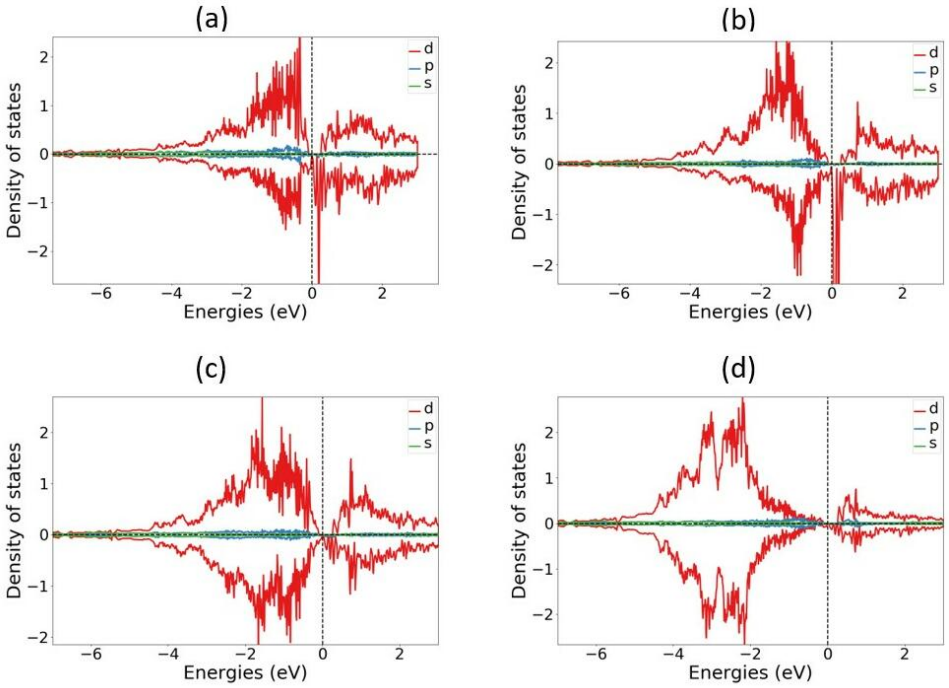

Figure 8.4: Local density of states of TMs (SQS D), (a) Cr, (b) Mn, (c) Fe, (d) Ni

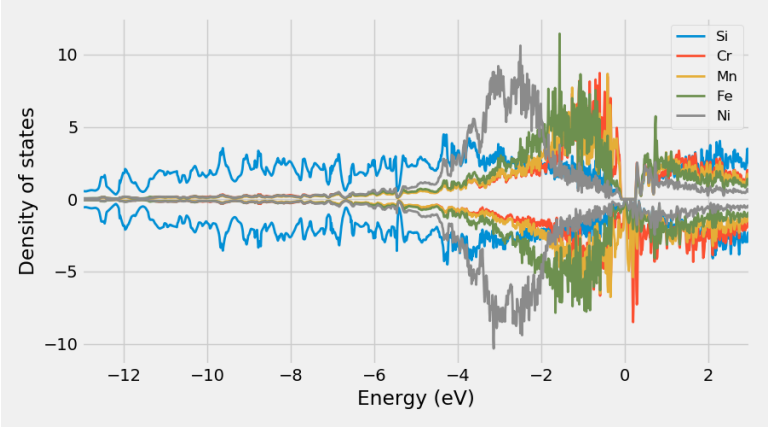

Figure 8.5: Projected density of states SQS D CFMN (fesi2) from PBE calculation

In agreement with the local DOS we observe here that the Si s-electrons occupy the lower energetic states, and evidence of p-3d hybridization at higher energies. With the upmost energetic states in the valence band occupied by 3d electrons of chromium and manganese. Bellow we include the PDOS of SQS D and B but focused around E_F, from these figures we find that the spin down channel in D contain a more dominant presence of manganese especially, and some chromium as compared to the semiconducting SQS B.

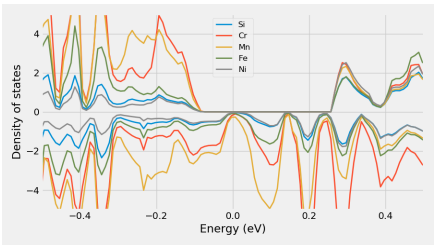

(a) Projected density of states of SQS D around E_f

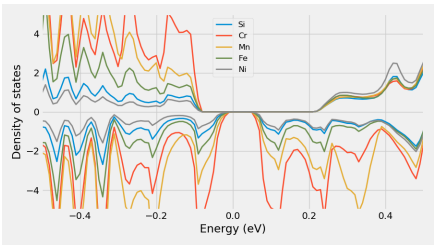

(b) Projected density of states of SQS B around E_f

In the context of DFT and VASP there are several factors than can affect the accuracy of the DOS. As mentioned in section .., the type of numerical smearing is paramount for accurate DOS calculations. In this project we experienced large differences between calculations from gaussian and TBC smearing in relation to the band gap and DOS, this will be covered in more detail later. Moreover the DOS is very sensitive to computational factors such as the number of points (NEDOS in VASP) and the number of k-points (to solve the DOS integral, see section ..). For example, the band gap in structure C could only be seen in the density of states when increasing the number of points in the DOS from 2401 to 20000 points. This is shown bellow in figure blabla, where we plot the density of states around the fermi energy, denoted by the strippled red and blue lines, relative to the density of states with 2401 points and 20000 points respectfully, all

other parameters remained unchanged, it should however be noted that the second calculations applied the charge density calculated by the former for quicker convergence.

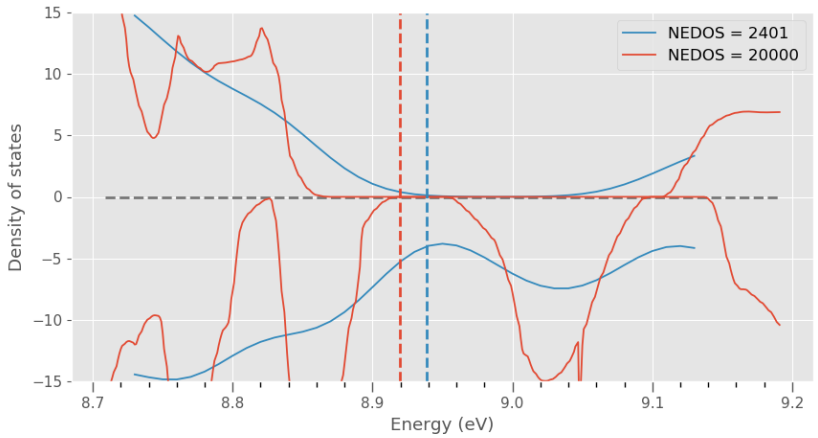

Figure 8.7: Density of states of SQS C with 2501 points vs 20000 points in the density of states.

Despite of the higher accuracy of the greater number of points, we continue to perform calculations with around 2400 points in most calculations, mostly down to the increased workload for analyzing and producing DOS figures with such a large number of points, and the use of vaspkit's tools.

The values listed in table 8.3 was calculated from the Kohn-Sham eigenvalues. In addition to validate and provide an additional measure to the density of states, we can qualitatively differentiate SQS D by looking at the eigenvalues. For certain k-points the occupancy does not transition from 1 to 0 directly between two bands, but rather contain one or more partially occupied bands in between (**Visualize? type fermi-dirc plot**), however only in the spin down channel. If we were to neglect these partially occupied states and only consider bands where the occupancy is above 0.99 or bellow 0.01, the band gap of structure D remain consistent in spin up, but we now observe a band gap of around 0.05 eV in the spin down channel resulting in a total band gap in the structure. Again, this would have been extremely insightful to investigate with the help of a band structure diagram.

8.1.3 Meta-GGA and hybrid functional

As expressed previously, in this work we invoke 3 level of depths GGA (PBE), meta-GGA (SCAN) and hybrid functionals (HSE06) to determine the band gap of the SQSs. In table .. bellow we list the respective band gaps of these methods for all 5 SQSs of CFMN (fesi2). Note that all calculations is done with TBC smearing.

Structure	PBE	SCAN	HSE06
A	0.0281	0.0000	0.0207
B	0.0523	0.0890	0.1808
C	0.0344	0.0690	0.0196
D	0.0000	0.0000	0.0000
E	0.0495	0.1048	0.0133

Table 8.4: Band gap of CFMN ($FeSi_2$) SQSs with GGA (PBE), meta-GGA (SCAN) and hybrid-functionals (HSE06).

Need a comment on why we use the SCAN functional exactly, answer: Considered accurate, fast, and allows for testing on a level between gga and hybrid. Write this in the method section.

The most obvious result of table .. is that aside from SQS A, all 3 methods agree on the presence of the band gap. This in itself is a very positive result for this project, as the primary motivation is based simply on locating semiconducting high-entropy silicides and thus the agreement of 3 different methods on the same structures is most welcome. On the other hand, it's clear that the actual size of the gap is under some debate. We note the largest observed band gaps is largely associated with the SCAN functional, compared to PBE calculations this result is very in line with what is expected by involving more complex factors in the calculations, as discussed in section .. In contrast, by the same argument we would not expect that par SQS B, the overall smallest band gaps is found with the well-proven hybrid functional HSE06, as shown in table .. The results associated with the HSE06 functional will be covered in more detail in the subsequent section, for now lets consider SCAN.

SCAN

For the most part, the results with SCAN meta-GGA prove similar to PBE, as was the case in the bulk material. The one exception is in SQS A. In this case the SCAN calculations result in a metallic character as opposed to the 0.03 eV band gap from PBE. Upon investigating we discover that the eigenstates is riddled with both partial occupancy and so-called non-physical values. If we were two neglect these, we find a band gap of 0.031 eV, very in line with the PBE result **Should I include this? I don't know why or what this means. And I don't really wanna spend a significant portion on one result with SCAN.**

Other noteworthy concerns about the SCAN functional is apparent in the results of SQS C and D. **Plot DOS C with PBE and SCAN side by side or like NEDOS around Ef to show the difference. Also make one for E to show how SCAN decrease the spin up gap and increase the spin down gap.**

HSE06

Wait for jobs to finish: lesssmear and ismear0 As stated above, the

measured band gaps with the HSE06 functional was less than that of PBE and SCAN for most of the tested SQSs. Hybrid functionals as described in section .. is computationally demanding, but comes with superior accuracy for band gap measurements, and the HSE06 functional in particular is on the top of the list. For this reason, one would in general expect larger band gaps compared to GGA or meta-GGA calculations, as highlighted in .. **cite?** The one exception we observed to this trend is in SQS B, here the band gap increase from 0.05 eV to 0.09 eV and 0.18 eV from PBE to SCAN to HSE06. One possible reason behind the abnormally large gap can originate from the small number of k-points we had to employ in order for the calculations to converge. Recalling that the gap transition in in the PBE calculation was (0.250,0.000,0.250)-(0.000,0.000,0.000), compared to the hybrid functional we now see that the transition is between k-points (0.500,0.000,0.000) and (0.000,0.000,0.000). Moreover, the point (0.250, 0.000, 0.250) in k-space is not included in the hybrid functional due to the narrow mesh (this we read from the IBZKIT file in VASP). Thus it's a possibility that the large gap is caused by the fact that the minimal gap is not encapsulated by the k-points in the HSE06 calculation. However we also see this trend in the other SQSs, but despite of the different transistion in k-space, these structures find lesser band gaps with the HSE06 functional compared to PBE. Additionally, we find similar results in the bulk $\beta-FeSi_2$ structure. In this calculation we applied the same number of k-points for HSE06 as for PBE and SCAN. Nevertheless we find a much larger band gap of around 1.5 eV with HSE06, as opposed to 0.65 eV with both PBE and SCAN, and as mentioned before the two latter is in much better agreement with experimental results and ab intio work on the band gap of $\beta-FeSi_2$ **cite materials project, other articles**. Additionally also in this case, the transition vary between functionals. PBE: (0.000,0.000,0.000)-(0.000,0.000,0.250), and HSE06: (0.000,0.000,0.000)-(0.000,0.000,0.500). **Include band-diagram for bulk fesi2?**

Aside from SQS B, we find generally good agreement between HSE06 and PBE calculations. In A we notice that the 0.02 eV band gap of tabel .. stems from a 0.7 eV gap in spin up and 0.02 eV in down. Likewise SQSs C, D, and E all exhibit large band gaps in spin up, 0.17, 0.37 and 0.55 eV respective, and corresponding very narrow gaps in spin down equal to 0.032, 0, and 0.013 eV. If we compare to the listed spin gaps from PBE in table .., we see that the band gaps of HSE06 typically compares or exceeds in spin up, and lessen in spin down, except in B (0.29 eV and 0.18 eV).

Include here a figure or number on the computation time between PBE, SCAN and HSE06. Figure comparing the DOS between PBE, SCAN, HSE06 for one SQS?

Rewrite/reconsider this paragraph, is it needed? How can I write this more concise? Figure? One final point we would like to cover in the discussion of HSE06 calculations of this system, and generally in this project, is the effect of smearing on the reported band gaps. From the method section, we know that TBC smearing is the preferred choice for accurate density of states and total energy calculations of semiconductors, alike we know that this method is unfitting to calculate the forces in metals. As discussed in the methodology section, hybrid functionals

proved difficult to converge for such composistionally complex structures, thus we were forced to initially calculate the charge density from the HSE06 functional with did a self-consistent calculation with gaussian smearing and smearing width of 0.05 eV. Thereafter reuse the calculated charge density for subsequent hybrid calculations with TBC smearing. Using SQS A as an example, from the first run (Gaussian), the band gap is 0.15 eV, (0.78 up and 0.15 down). However the eigenvalues contain defect states and the band gap is not observable from the density of states. Next we can reapply the charge density to perform an additional HSE06 calculation with gaussian smearing, but reducing the smearing width from 0.05 eV to 0.005 eV. Now we find a new gap of 0.1 eV (0.21 up and 0.1 down), with no defects in the eigenstates, and apperant in the density of states. In cases where we find conflicting results between the eigenvalues and density of states we rely on the script bandgap.py provided in the pymatgen package, refer to section .. for a description. With this we only report a band gap for the HSE06 calculation with TBC smearing, note that this method return the same value of the gap as well. As another example lets consider SQS B. In contrast, the nummerical smearing does not appear to impact the band gap of this structure. We find from HSE06 simulations with gaussian smearing of both 0.05 and 0.005 eV smearing width to yield results around 0.28 eV and 0.18 eV in spin up and down. But alike SQS A, the larger smearing width comes with a few defect states in the spin down channel and additionally can not be seen in the density of states. However, particular of this structure is that the bandgap.py script validate the calculated total band gap from the eigenvalues in all three calculations. Aside from this abnormalty, the other SQS similar to A find some similarities between smearings, but only TBC was validated with bandgap.py, furthermore the DOS does not with the same clarity reproduce the calculated band gap from the eigenvalues in calculations done with gaussian smearing compared to TBC. **Create figure/subfigure of the DOS of hybrid/smear/smear5 calculations to illustrate the above point, maybe A**

We see from the above examples that as most studies and articles state, that TBC smearing is superior in terms of accurate total energy and DOS calculations of semiconductors. Similar to how TBC produce inacurate forces of metals, in several cases in this project we relaxed the structures with gaussian to forces bellow 1E-2, but subsequent calculation with TBC in certain cases resulted in forces above 0.1, without making any geometric alteration to the previously relaxed cell **(Include examples?)**. On the grounds of these factors we can report good agreement between our own results and the theoretical advice regarding numerical smearing in DFT studies **Insert refrences**

We see that the band gap of the high-entropy silicide vary between both PBE, SCAN and HSE06. From the SCAN functional we found several cases that disagreeed with the PBE results, see SQS A, C and D. Combining this with the popularity and wide-spread application and reliability of the PBE functional. See for example materials project, that exclusivly list PBE band gaps, and other relevant studies **refrences**. We put the most faith in the

PBE results. An additional point is that GGA is known to underestimate band gaps, due to the concepts described in section .., therefore if we find a gap with PBE, the real material would most probably also have a band gap, and a larger one at that.

Regarding the HSE06 functional, the inaccuracy shown for the bulk material is concering, escpecially considering the lack of experimental baselines in this study to compare and measure our results after. However, generally we find much better cohesion between PBE and HSE06 compared to SCAN for the 5 supercells, both methods predict semiconductors with heavy spin polarization in the spin up direction, par B. The fact that all 3 functionals and five structures for the most part agree on the presence of a semiconductor is a overwhelmingly positive result in itself, that allow us to state with high certainity that this compound is in fact a semiconductor, or we may label the compound as a half-metal or spin-gapless conductor from the registered spin dependence. A qualitative study on the exact band gap would demand a much greater scope as there are many factors affecting the value that we have neglected. One of these is the randomness involved with SQSs. For instance, by increasing the SQS size, ie number of atoms in the supercell, we found again different band gaps, but still, the presence and characther of the compound was consistent. **Include this? Table?** To draw any meaningfull conclusions on the size of the band gap would requiere us to both increase the number of SQS's of the composistion due to the obseved variation in the band gap between the 5 tested supercells, and as well for different supercell sizes to obtain some sort of convergence of the band gap. On the other hand, if we go by the most stable configuration, then this compound would be labeled as a half-metal from the results of SQS D.

8.1.4 Probability distribution functions and charge density

In this final segment on the CFMN (fesi2) alloys we will include the probability distribution functions and charge density, which will be usefull for later comparisons. We only include the results of SQS B and D in this section, as we saw little variation across the five SQSs.

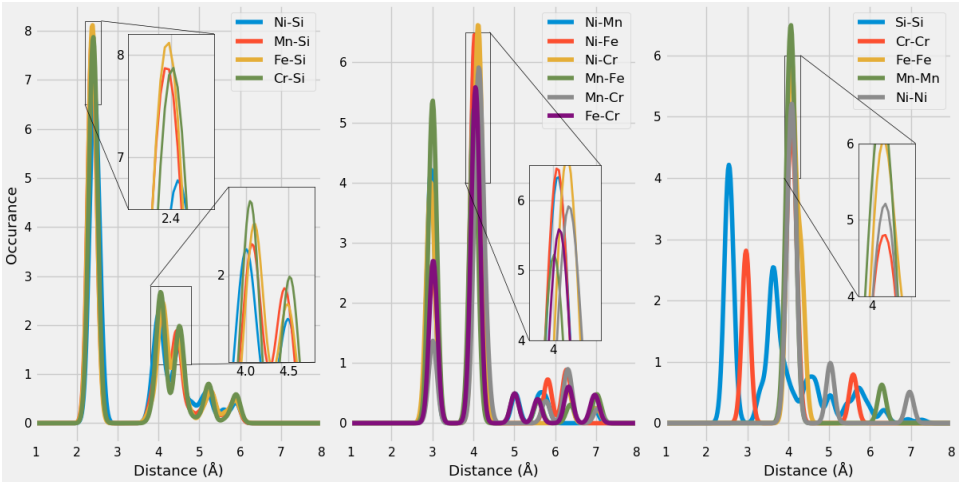

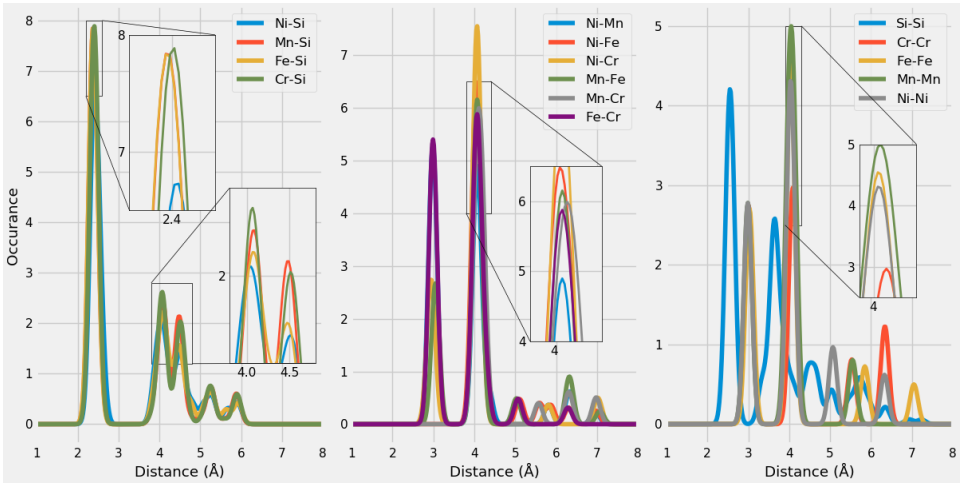

From these figures there is a lot of useful information to extract. With the aid of the ICSD (insert citation), we can compare the values of figure .. to the expected PDFs based on a number of experiments from a host of different compounds. As our compound contain a total of 15 different bonds, comparing each one to the ICSD values would be an exhaustive process. For our purpose we are satisfied by comparing the 4 different metal-Si bonds and note ourselves of key distinctions. We find that the preferred bond-length of TM-Si is observed at two values, the most dominant being the shorter of the two. For Fe-Si these are between 2.25-2.75 and 4-5, Mn-Si 2.25-2.75 and 3.5-5. Ni-Si lie between 2.25-2.5 and 3.85-5 and Cr-Si between 2.35-2.65 and 4-5. Clearly, the PDFs of the alloys are in good agreement with the listed values for Tm-Si bonds, with the most occurring bond length falling at around 2.4 Å for all TMs, and lesser occurrence between 4.0 - 4.5 Å. The relative height of the peaks follow a similar trend, Fe-Si, Mn-Si, and Cr-Si all lie close to 8 for the first peak at 2.4 Å, and Ni-Si slightly bellow around 7. Moreover we note that the Fe-Si occurance at 2.4 Å is lower in SQS B compared to D **More on the PDFs?**

Bellow we show the calculated charge density (from PBE) of structure B (left) and D (rights).

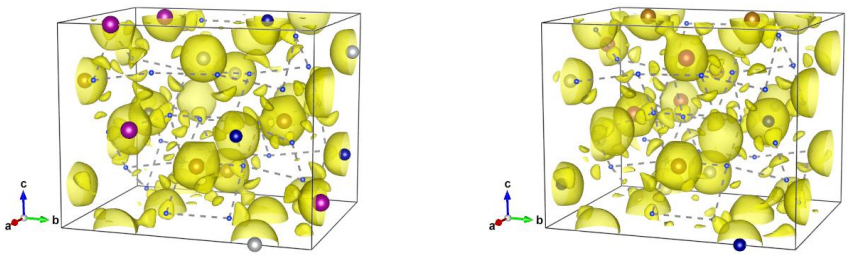

(a) Structure B

(b) Structure D

8.2 Permutations

Analyze LDOS, PDFs and CHGCAR of some SQSs

Up until this point we have investigated the structure CFMN ($FeSi_2$). More specifically we have looked at the center of a quasiternary pahse diargram. In this section, we aim to exapand our search of this diargram by generating SQSs slightly away from eqvimolar distribution of 3d elements. In table (bellow) we list the mean total energy and magnetic moment per atom with standard deviation and the enthalpy of formation of 4 permutations of the CFMN (fesi2) compound. Ideally we would alter one element at a time, but the TDEP implementation insist in also reducing Nickel to stay consistent with the 48 atom supercells. Thus we reduce Ni and one additional element per permutation.

	Toten (eV)		Enthalpy of formation	Mag	
$Cr_3Fe_3Mn_7Ni_3Si_{32}$	6.6947	0.0040	-11.9586	0.1375	0.0186
$Cr_5Fe_5Mn_3Ni_3Si_{32}$	6.6705	0.0030	-11.1991	0.1127	0.0223
$Cr_5Fe_3Mn_5Ni_3Si_{32}$	6.6852	0.0041	-10.5200	0.1375	0.0456
$Cr_3Fe_5Mn_5Ni_3Si_{32}$	6.6801	0.0036	-12.6426	0.0937	0.0209

Table 8.5: Mean and stadard deviation of the total energy and magnetic moment per atom, plus enthalpy of formation of the listed mean energies ($FeSi_2$).

The first result of table .. we make notice of is that the stability, as evaluated by the enthalpy of formation can be increased beyond the eqvimolar composition. This is accomplished in two distinct permutations, one with increments to manganese relative to the other TM, and the other by reduction of chromium. Moreover the two respective permutations lie on the opposite side of the magnetic scale. The large magnetic moment of the manganese rich permutation and the low magnetic moment in the chromium poor permutation is very much in line with the observations made in the previous section. Recalling that in the magnetic moment in the eqvimolar composition was largely attributed to manganese and chromium atoms in the lattice. Thus increments to manganese or reduction of chromium would following impact the magnetic moment as in the two permutations. For this reason, additionally the permutation $Cr_5Fe_3Mn_5Ni_3Si_{32}$ where the nonmagnetic elements is reduced and the magnetic elements are increased ,is equally magnetic. We however find no direct relation between stability and magnetism as his particular permutation is the least stable. An important property of table 8.5 is that the listed values are the mean value of the observed property for 5 distinct SQSs of the same permutation. For example we notice that while the highest magnetic moment in the first permutation is associated with the most stable SQS (from total energy considerations). The least stable supercell show the highest magnetic moment in $Cr_5Fe_3Mn_5Ni_3Si_{32}$.

The respective band gap of the permutations (with PBE) can be seen

in table ... Compared to the previous case, we find most SQSs of the permutations to exhibit a half-metallic character.

		Spin up (eV)	Spin down (eV)	Total (eV)
$\mathbf{Cr_3Fe_3Mn_7Ni_3Si_{32}}$	A	0.3390	0	0
	B	0.4745	0	0
	C	0.1342	0	0
	D	0.1950	0.0063	0.0063
	E	0.4211	0	0
$\mathbf{Cr_5Fe_5Mn_3Ni_3Si_{32}}$	C	0.2103	0	0
	D	0.0674	0.0413	0.0372
	E	0.3619	0	0
$\mathbf{Cr_5Fe_3Mn_5Ni_3Si_{32}}$	A	0.2082	0	0
	B	0.4053	0	0
	C	0.4659	0	0
	D	0.0843	0.0121	0.0121
	E	0.3008	0	0
$\mathbf{Cr_3Fe_5Mn_5Ni_3Si_{32}}$	A	0.3922	0	0
	C	0.1285	0	0
	D	0.2595	0.1004	1.004
	E	0.3591	0.1003	0.0848

Table 8.6: Total and spin dependent band gap of 4 permutations of CFMN (fesi2) with PBE GGA calculation. The structures that are excluded from this list either failed in calculations, or does not show any band gap. **Remove C and E from Mn3, these contain defects and no gap in DOS.**

From table .. we see that likewise to the stability and magnetization also the band gap changes in the different directions. To some degree we find positive results of the band gap in each direction, but we see particularly that permutations rich in manganese provide very encouraging results. This is made clear from the fact that $Cr_3Fe_3Mn_7Ni_3Si_{32}$, $Cr_5Fe_3Mn_5Ni_3Si_{32}$ and $Cr_3Fe_5Mn_5Ni_3Si_{32}$ all include amounts of manganese higher than the eqvimolar composistion and all associated SQSs show at least strong half-metalic charachter or semiconducting. On the other side $Cr_5Fe_5Mn_3Ni_3Si_{32}$ is the sole permutation with less manganse and correspondingly show the least sign of a band gap. Moreover the relative stability of the SQSs give further merit to the proposition. In the first permutation we find that the highest total energy is associated with SQS B, which as seen in table .. exhibit the largest spin up band gap of the particular permutation. Furthermore the two semiconducting SQSs in the last permutation is the two most stable arrangements. Reversely, in the manganese-poor permutation we find that the sole semiconducting SQS is the second least stable of that compound. Lastly, the opposite is the case is true in the third permutation. Despite the total energy not varying tremendously between SQSs of the same permutation, as seen by the standard deviation in table ..,

the continuing trend between stability and band gap is a promising result to report. Bellow we include the projected density of states around E_F of the 4 permutations for the most stable SQSs. Note that away from the fermi energy the projected density of states is very similar to the eqvimolar distribution, see appendix ..

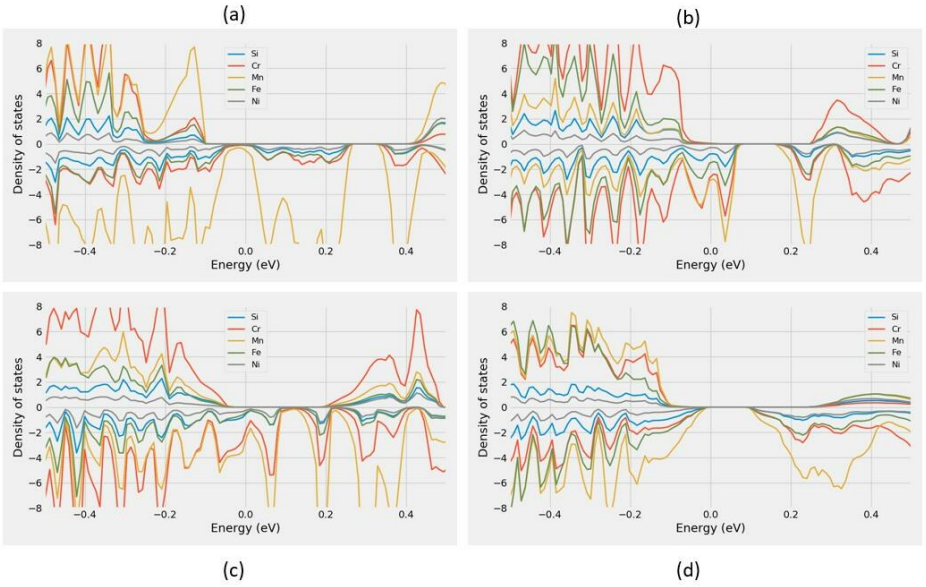

Figure 8.9: Projected density of states of (a) $Cr_3Fe_3Mn_7Ni_3Si_{32}$, (b) $Cr_5Fe_5Mn_3Ni_3Si_{32}$, (c) $Cr_5Fe_3Mn_5Ni_3Si_{32}$, (d) $Cr_3Fe_5Mn_5Ni_3Si_{32}$

Comment on the plot However, we could ask the question if the half-metal results is truly a good indication. In the previous section we learned that all though the SQSs of the eqvimolar system favored the spin up channel in terms of a band gap, the structures were still narrow semiconductors, and with relatively lesser amount of manganese. It's important to note however, that in this analysis we didn't just increase/reduce manganese, we simultaneously altered the other elements as well. Therefore we can not conclude that this or that is the best direction, but from exclusively the permutations we tested there is clear indication that manganese is related to the band gap in a positive way.

In this segment of the project we scarcely applied the more advanced functionals SCAN and HSE06, in part to both the uncertainties mentioned in the previous section and the computational cost of the methods. However we did perform such calculations (HSE06) to further investigate the nature of the listed semiconducting SQSs. Both the manganese rich and poor semiconductors are validated with the HSE06 functional and find wider band gaps of 0.17 eV (0.57 and 0.26 in up and down) for the manganese rich composition, and 0.22 eV (0.77 eV in spin up) for the manganese poor composition. On the opposite side, the very narrow band gap of SQS D in the third permutation vanishes with HSE06 calculations. For the two stable semiconductors found in the reduced

chromium permutation, simulations with the HSE06 functional resulted in a half-metal gap in spin up of 0.53 eV for SQS D, and a total band-gap of 0.27 eV for E, where the spin-up gap is 0.73 eV wide.

In future research, it would be interesting to deliberately alter specific combinations from the results of table 8.6, for example reducing chromium and increasing manganese simultaneously.

Chapter 9

The bad (Other compositions of the $FeSi_2$ unit cell)

Include results for CRFeMnCo to finish! In similar fashion to the previous sections, we here begin by presenting the mean and standard deviation of the total energy and magnetization of a set of SQSs corresponding to different high-entropy silicides of the $Fesi_2$ unit cell. The compositions we have tested are deliberate combinations intended to investigate both the impact of manganese by replacing the element with Co or Ti, and concepts related to HEA theory such as the atomic size effect. Furthermore Co is a very common element in many stable HEA, as seen in section .., thus we include two (3?) compositions with this element to study the impact on stability and the functional properties. The results of the aforementioned alloys can be seen bellow in table 9.1, note that all compounds contain a total of 48 atoms as before.

	Toten (eV)		Enthalpy of formation	Mag	
$Cr_4Fe_4Co_4Ni_4Si_{32}$	- 6.4655	0.0056	-12.7536	0.0083	0.0155
$Co_4Fe_4Mn_4Ni_4Si_{32}$	- 6.4731	0.0046	-15.0836	0.0000	0.0000
$Cr_4Fe_4Ti_4Ni_4Si_{32}$	- 6.4217	0.0087	-7.5040	0.0305	0.0293
$Cr_4Fe_4Mn_4Ti_4Si_{32}$	-6.6994	0.0071	-7.3060	0.1142	0.0641

Table 9.1: Summary of the total energy, enthalpy of formation and magnetization of several composistionally different SQS high-entropy alloys based on the $\beta-$ $FeSi_2$ unit cell.

Maybe discuss the std of mag and relation to energy of sqs, several cases we find large differences between SQSs. From table 9.1 we see that the stability of the relative compositions vary greatly. By introducing cobalt to the alloys, particularly at the cost of manganese result in a large positive effect on the stability, contrary replacing either manganese or nickel with titanium significantly lowers the stability. In terms of the magnetization, the results are in line with the observations of the CFMN composition, from table 9.1 it's clear that replacing either manganese or chromium drastically reduces the magnetization of the alloys. In addition, we find

indication of chromium being further significant to the magnetization than manganese as seen from the first and second compounds in table 9.1 respectively. In opposition to the study of the CFMN system we observe here a clear relation between magnetization and stability. However, we are not confident if the observed outcome is a direct consequence of the magnetization or simply a product of addition of cobalt and titanium respectively to the alloys. On the other hand, in both cases the least magnetic composition is also the most unstable, thus there is weight behind the magnetic relation to stability. **Wait for CrFeMnCoSi2 to finish**

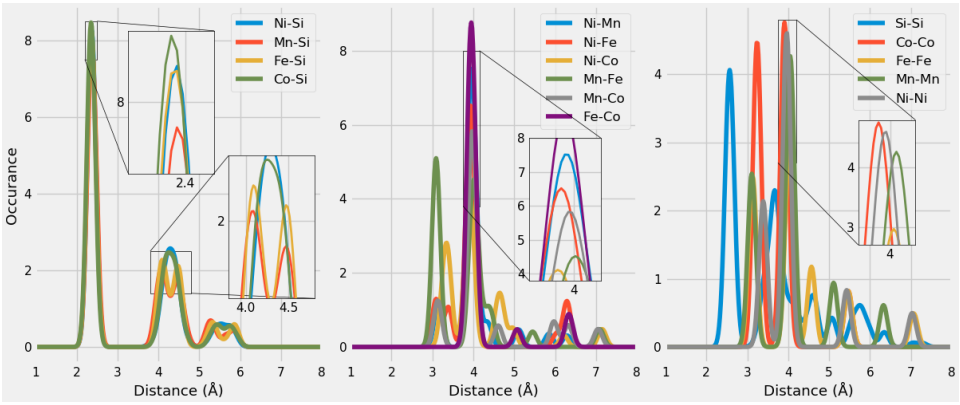

Figure 9.1: Probability distribution function $Co_4Fe_4Mn_4Ni_4Si_{32}$ (SQS (D))

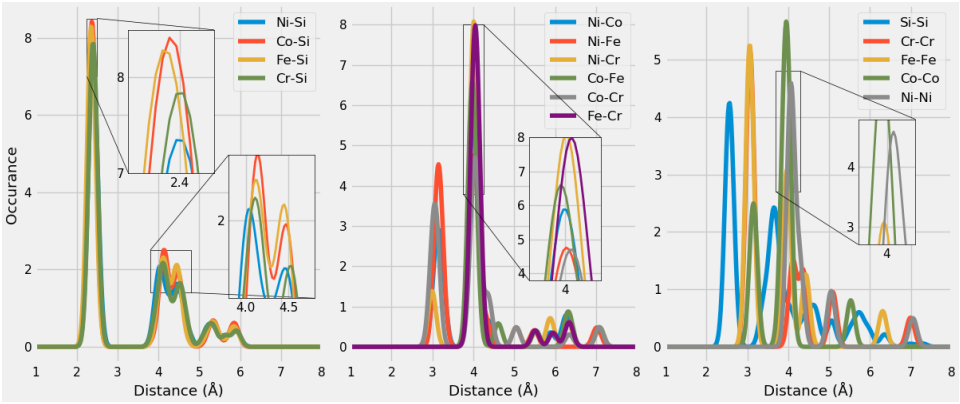

Figure 9.2: Probability distribution function $Cr_4Fe_4Co_4Ni_4Si_{32}$ (SQS (B))

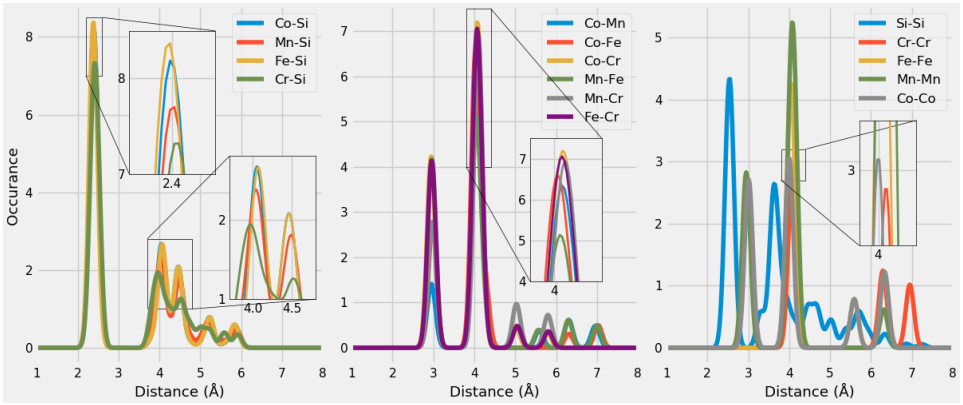

Figure 9.3: Probability distribution function $Cr_4Fe_4Mn_4Co_4Si_{32}$ (SQS (B))

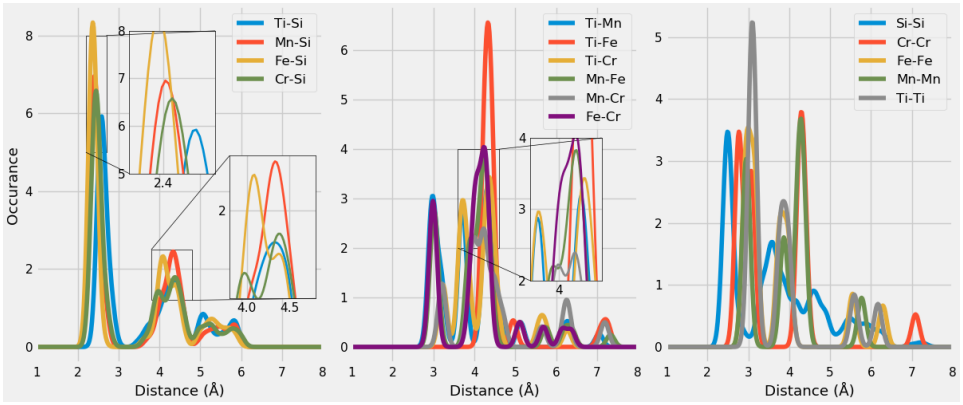

Figure 9.4: Probability distribution function $Cr_4Fe_4Mn_4Ti_4Si_{32}$ (SQS (B))

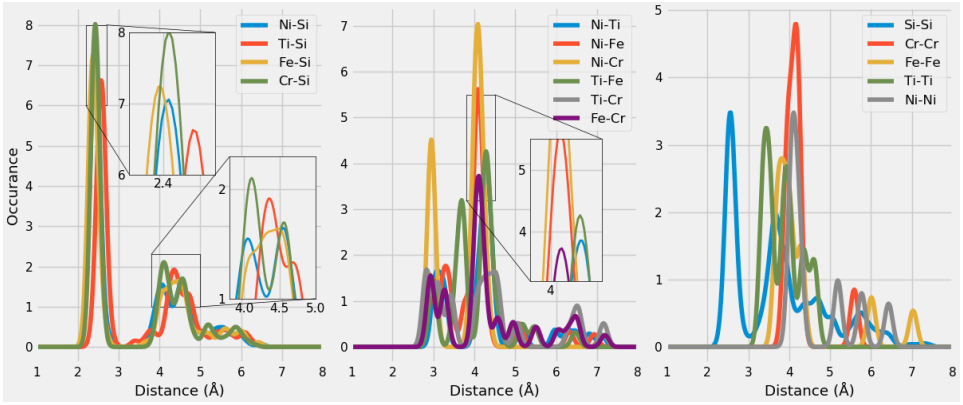

Figure 9.5: Probability distribution function $Cr_4Fe_4Ti_4Ni_4Si_{32}$ (SQS (B))

Insert figures related to the band gap, stability to band gap results, which SQS of each compo is most stable

In regards to the band gap of the compositions, we can report that a heavy majority are metals. We found no evidence of a band gap in both the CrFeCoNiSi2 and CrFeMnTiSi2 alloys across all supercells, as seen in the

density of states of the two most stable SQSs of the respective compounds **Add figures**. Further also the most stable SQSs of the CrFeTiNiSi alloy point to a metal. Similarly the most stable SQSs of the CoFeMnNiSi2 alloy are clearly metals. Noteworthy of this composition however is that we find clear evidence of a narrow band gap in two SQSs (A and B). In terms of stability, these lie around the mean total energy of the set. The respective band gaps are 0.033 eV in A and 0.0058 eV in B. **Include DOS or other figures for these results.**

To follow is details on the gaps in A and B, is it worth to include this? In the density of states plotted in figure .., the band gap in A is clearly visible. On the other hand the very narrow gap in B is not as apparent, as the states around Ef contain very small nonzero values. This could be related to the low resolution of 2500 points in the density of states as seen before, especially considering the size of the gap. In opposite to the CFMN calculations previous we here experience excellent cohesion between PBE and SCAN simulations on the band gap. With the meta-GGA functional the band gap of SQS A and B respective is 0.04 eV and the 0.003 eV. Moreover we find the identical gap transition with both functionals, which was not the case in previous endeavors with this functional. Additionally we also find that the HSE06 functional produce dissimilar results to previous experiences. In this scenario, the HSE06 functional fails to recognize the observed band gap of PBE and SCAN in both supercells. The greater number of k-points in the GGA and meta-GGA calculations offer more accurate band gaps, however lesser k-points will not result in a smaller gap, only bigger. Thus the uncertainites of previous calculations of the HSE06 functional does not apply in this case. For this reason in addition to the reputation of hybrid functionals and the lack of other factors to negatively affect the validity of the result, we find it challenging to conclude on the band gap of these structures between functionals.

Part IV

Conclusion

Write conclusion here